

## **Hydrodynamic Study of Wave Evolution Characteristics around Semi-Submersible Platform in Shallow Water with Submerged Terrain near Island**

*Ke Xia, Yong Ai, Decheng Wan\**

Collaborative Innovation Center for Advanced Ship and Deep-Sea Exploration, State Key Laboratory of Ocean Engineering,  
School of Naval Architecture, Ocean and Civil Engineering, Shanghai Jiao Tong University, Shanghai, China

\*Corresponding author

### **ABSTRACT**

In the present study, our in-house 3D viscous flow solver (naoe-FOAM-SJTU) is employed to simulate the wave evolution characteristics and hydrodynamic properties of semi-submersible platform in the corresponding wave environment in shallow water with submerged terrain near island. The validation work was done by comparing the RAO (Response Amplitude Operator) of numerical results with experimental test data conducted by Tian et al. (2014) which shows great correlation. The profile and properties of the wave evolution, breaking and the hydrodynamic characteristics of the floating platform over the submerged terrain are clearly depicted with different wave steepness in this study.

**KEY WORDS:** Wave evolution; semi-submersible platform; submerged terrain; wave steepness; naoe-FOAM-SJTU solver.

### **INTRODUCTION**

With the rapid development of the ocean resources, more and more attention are drawn to the islands and reefs. Various supplies are indispensable in the process of construction and development of the islands. Hence, it's suitable to build a semi-submersible platform for guarantee. Whereas, wave environment is relatively intricacy (wave diffraction, reflection, wave turning and wave breaking) in the shallow water with the effect of submerged terrain. According to the wave environment, the hydrodynamic response of the platform is absolutely disparate from that in the deep sea.

The investigations about floating structures have been conducted for a relatively long time, and several methods were adopted to research the hydrodynamic characteristics of the semi-submersible platform. A reasonable assumption is put forward by Morison (1950) that a semi-empirical formula can be adopted in the calculation of wave force upon marine structure and wave force around the platform can be classified into two parts including inertia force and drag force. This formula is widely used in the calculation of small scale component of the platform whose cross section is relatively simple (Lee and Incecik, 2005). Maeda et al. (1992) investigated the motion response of a semi-submersible platform in certain directional regular waves and they found that

viscous effects are very prominent in certain frequency ranges of incident waves which dominate the steady drift force and low-frequency drift motions of platform. Comparisons with experimental result showed good agreement only if the viscous effects were well considered. A similar observation had been made earlier by Kobayashi et al. (1987) with regard to the surge motions of a TLP. Donley and Spanos (1992) presented a method to study TLP response including the effects of potential and viscous drift forces. In that study, the viscous force of drag was calculated up to the mean water level using the statistical quadratization procedure. Although numerous studies have been conducted to depict the hydrodynamic characteristics of floating structures, most of the researches about the response of floating platform were primarily focused on the deep sea area. A relatively small part of researchers focus their attention on the hydrodynamic response of structures in shallow water. Tian et al. (2014) took a certain island and floating platform near island as the research object in study, and the characteristic of wave propagation near island and the influence of island on motion responses of platform were analyzed by hydrodynamic model tests. Ding et al. (2014) conducted a numerical research based on the Morison formula and finite water depth Green function, in which the motion and load response characteristics of a semi-submersible near island are studied, the wave frequency responses and second order wave forces of platform in various wave directions and water depths were calculated, and the corresponding long-term prediction of mid-ship section vertical bending moment was also obtained.

The wave environment in shallow water is more intricacy which is absolutely different from that of deep sea. The wave propagation is always been affected by the submerged terrain in which linear wave theory cannot be used in the hydrodynamic study of floating structures. A series of wave evolution phenomenon, such as wave diffraction, reflection, refraction, would be caused by the limitation of seabed. Some strongly nonlinear phenomenon such as wave turning and breaking would also occur in this process. Herein, the wave evolution and corresponding research methods should be also investigated in the study of floating structures in shallow water.

Wave evolution and breaking in shallow water with different water depth and angle of slope is a significant subject in coastal and marine engineering. It is a two phase flow phenomenon involving air and water,

and it strongly influence the air-water interaction by enhancing momentum and energy transfer between two phases, which thereby limits the wave steepness, generating vorticity and turbulence, enhancing wave energy dissipation, entraining air and white water formation (Chella et al., 2015). According to the dispersion relation, the wave velocity and the wave length decrease with the reduction of the water depth in the process of wave propagation shoreward. Hence, the velocity of the front part is smaller than the rear part, which related to the wave energy accumulate upward with the shorter wave length, and the wave height increase which leads to the wave evolution in this process. When the steepness ( $H/L$ ) is too large and exceed the limitation, the wave breaking occurs.

Numerous studies have attempted to explain the wave evolution and breaking process and their characteristics. The detailed literature review on wave breaking in deep and shallow water can be found in Cokelet (1977), Peregrine (1983), Basco (1985), Banner and Peregrine (1993), and Perlin et al. (2013). In the case of submerged terrain and reefs, wave breaking is strongly influenced by the local environmental parameters, such as water depth ( $d$ ) and sea bed slope ( $m$ ). This has been studied in laboratory experiments by Blenkinsopp and Chaplin (2008). In order to research the nonlinear phenomenon, several surface wave theories have been investigated and proposed to resolve the wave breaking issues. Meanwhile, many theories were put forward to describe the wave breaking, and most studies in the field of submerged breakwater structures have only focused on the prediction of the reflection and transmission characteristics of waves for a given environmental condition. Ting and Kim (1994) investigated the wave transformation over a submerged structure and concluded that potential theory cannot be applied to model the flow process such as flow separation and energy dissipation. However, the breaking process and generation and dissipation of vortices are created by rotational flow (Takikawa et al., 1997). Numerical modeling of wave breaking becomes challenging due to the intricacy in describing the physical processes involved such air-sea interaction, vorticity generation, overturning motion and the air entrainment. Hence, a straightforward approach to describing the breaking process numerically is applied to solve the fundamental fluid dynamic equations with CFD (Computational Fluid Dynamics) method. Chella et al. (2015) did the investigation about the characteristics and profile asymmetry properties of wave breaking over an impermeable submerged reef by the CFD method, and the capture of free surface is conducted by the level set method. The numerical result showed great correlation to the experimental results which is just the contribution of consideration of vortex and viscous.

In this paper, our in-house three-dimensional (3D) viscous flow solver (naoe-FOAM-SJTU) which is developed and based on the popular open source toolbox OpenFOAM for predicting dynamics of floating structures with mooring systems is presented. The hydrodynamic response of semi-submersible platform is primarily investigated in the shallow water environment in which the influence of submerged terrain is well considered. Herein, the wave evolution characteristic of different waves are also observed, and the effect of wave steepness to wave evolution characteristic and wave breaking phenomenon is also studied. The present numerical results of RAO (Response Amplitude Operator) were compared with the AQWA results and experimental results that conducted by Jiangsu University of Science and Technology's wind/wave current basin, located in Zhenjiang, China (Tian, 2014). The computed results show great agreement with the experimental data. The wave evolution phenomenon and the effect of wave steepness upon the wave evolution characteristic and wave loads on platform were discussed in detail.

## NUMERICAL METHODS

The present solver naoe-FOAM-SJTU (Shen et al., 2014) adopted for numerical simulation is based on a built-in solver in OpenFOAM named interDyFoam, which can be used to solve two-phase flow which is incompressible, isothermal and immiscible. To deal with common fluid-structure interaction problems in ship hydrodynamics and offshore engineering, several modules are further developed and integrated into the solver, such as a wave generation/damping module, a six-degrees-of-freedom (6 DOF) module and a mooring system module. Laminar Reynolds model are carried out in all the calculations. Mathematical formulae related to the solver are described as follows in detail.

### Governing equations

For transient, incompressible and viscous fluid, flow problems are governed by Navier-Stokes equations:

$$\nabla \cdot \mathbf{U} = 0 \quad (1)$$

$$\frac{\partial \rho \mathbf{U}}{\partial t} + \nabla(\rho(\mathbf{U} - \mathbf{U}_g)\mathbf{U}) = -\nabla p_d - \mathbf{g} \cdot \mathbf{x} \nabla \rho + \nabla(\mu \nabla \mathbf{U}) + \mathbf{f}_\sigma \quad (2)$$

Where  $\mathbf{U}$  and  $\mathbf{U}_g$  represent velocity of flow field and grid nodes separately;  $p_d = p - \rho \mathbf{g} \cdot \mathbf{x}$  is dynamic pressure of flow field by subtracting the hydrostatic part from total pressure  $p$ ;  $\mathbf{g}$ ,  $\rho$  and  $\mu$  denote the gravity acceleration vector, density and dynamic viscosity of fluid respectively;  $\mathbf{f}_\sigma$  is the source item. The laminar model was adopted in this study. The laminar model means that the Navier-Stokes equation will be solved directly and the turbulence model is not been considered in the calculation.

### Wave generation and relaxation zone

Wave generation is a vital part for the investigation of floating offshore structures and wave evolution. The wave generation and wave damping work are implemented by an open-source toolbox for CFD library: waves2foam. The wave was generated by modification of the velocity boundary condition and the phase boundary condition. In this study, Stokes 2<sup>nd</sup> wave theory was adopted in the g0eneration of the wave according to the calculated wave cases. The equation of Stokes 2<sup>nd</sup> wave theory was below:

$$\eta = \eta_1 + \eta_2 \quad (3)$$

$$\eta_1 = \frac{H}{2} \cos \omega t \quad (4)$$

$$\eta_2 = \frac{\pi H^2}{8L} \frac{\cosh kd}{\sinh^3 kd} (2 + \cosh 2kd) \cos 2\omega t \quad (5)$$

In which,  $\eta$  is the wave elevation of free surface in certain point, and  $H$  is wave height of the generated wave,  $k$  is the wave number and  $d$  is the water depth at the local position.

In this wave maker module, relaxation zones are implemented to absorb the incident wave that keeps mass conservation and avoids reflection of

waves from outlet boundaries at the same time and what else to avoid waves reflected internally in the computational domain to interfere with the floating structure and wave maker boundaries. The former obviously contaminates the results, and the latter is found to create discontinuities in the surface elevation at the wave making boundary, which leads to divergent solutions (Jacobsen et al., 2012). A relaxation function

$$\alpha_R(\chi_R) = 1 - \frac{\exp(\chi_R^{3.5}) - 1}{\exp(1) - 1} \quad \text{for } \chi_R \in [0, 1] \quad (6)$$

is applied inside the relaxation zone in the following way

$$\phi = \alpha_R \phi_{\text{computed}} + (1 - \alpha_R) \phi_{\text{target}} \quad (7)$$

in which  $\phi$  is either velocity of phase indices. The definition of  $\chi_R$  is such that  $\alpha_R$  is always 1 at the interface between the non-relaxed part of the computational domain and the relaxation zone, as illustrated in Fig.1.

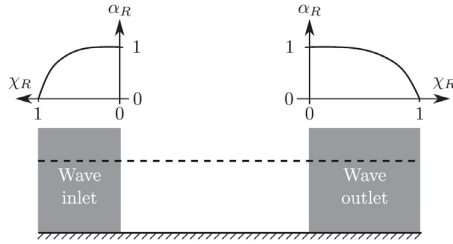


Fig. 1. A sketch of the variation of  $\chi_R$  for both inlet and outlet relaxation zones (Jacobsen et al., 2012).

### Mooring system

To simulate the actual condition and the interaction problem of the mooring line and floating platform, the code of mooring line module is developed and added to the existing solver. The mooring line used in this paper is based on the PEM (piecewise extrapolating method) which is implemented to calculating the statics of mooring lines and it could take into account line elongation as well as the drag force induced by the fluid. It is a quasi-dynamic method and in this method, mooring lines are divided into a number of segments, and a typical example of these is shown in Fig. 2. Equations of static equilibrium are established in both horizontal and vertical directions:

$$\begin{cases} T_{xi+1} = T_{xi} + F_i ds \cos \varphi_{i+1} + D_i ds \sin \varphi_{i+1} \\ T_{zi+1} + D_i ds \cos \varphi_{i+1} = T_{zi} + F_i ds \sin \varphi_{i+1} + w_i dl \end{cases} \quad (7)$$

Where  $T_x$ ,  $T_z$  and  $\varphi$  represent horizontal and vertical components of tension at a cross section of one segment and the angle between tension and  $T_x$ ;  $dl$  and  $ds$  are length of the segment before and after elongation respectively;  $w_i$  is net submerged weight of lines per unit length;  $D$  and  $F$  denote normal and tangential components of drag force acting on the segment which are calculated by Morison's equation.

In the naoe-FOAM-SJTU solver, the fluid force is calculated by solving the N-S equation, and the mooring force was calculated by the PEM.

Finally, the two forces will be added with body force to get a total force which can be used to solve the 6-DOF equation and to get the displacement and velocity of the floating structure (Shen et al., 2014). The development of PEM and validity has been validated by Liu et al. (2015).

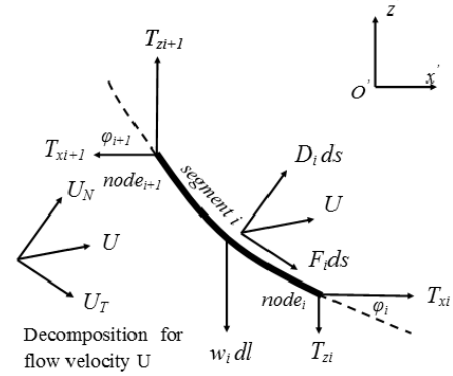


Fig. 2. Force analysis of a mooring line segment for PEM.

## COMPUTATIONAL DOMIAN, CASES AND PARAMETERS

### Platform parameter and mooring system configuration

The semi-submersible platform is composed of three cuboid pontoons, six oval columns and a box-shaped upper deck. As seen in Fig. 3, the calculated model is absolutely identical with the experimental model which is conducted by Tian (2014). And the gross parameters of the semi-submersible platform is shown in Table 1.

Table 1. Gross parameters of semi-submersible platform

Primary parameter	Unit	Value
Length of platform	m	50
Breadth of platform	m	25
Depth of platform	m	9.7
Draft below SWL4	m	5
Displacement	m <sup>3</sup>	2970
Center of mass location above SWL along platform center line	m	1.01
Platform roll inertia about center of mass (CM)	Kg · m <sup>2</sup>	7.67 × 10 <sup>8</sup>
Platform pitch inertia about center of mass (CM)	Kg · m <sup>2</sup>	2.29 × 10 <sup>8</sup>
Platform yaw inertia about platform centerline	Kg · m <sup>2</sup>	8.73 × 10 <sup>8</sup>

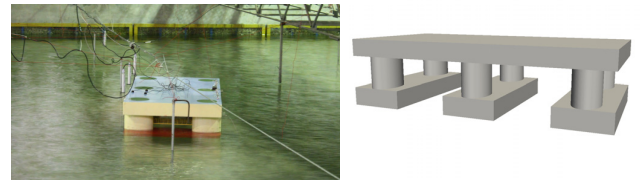


Fig. 3. Overview of experimental (left) and numerical model (right).

The mooring system was made up of eight mooring lines, and the angle between each group is 150.1 degree or 14.9 degree. The angle between the two mooring lines in identical group is 7.5 degree. The water depth of local area is 10 m, and as seen in Fig.4, the configuration of mooring lines is asymmetry for the consideration of the irregular slope of the submerged terrain. The parameters of the mooring system in detail are shown in Table 2.

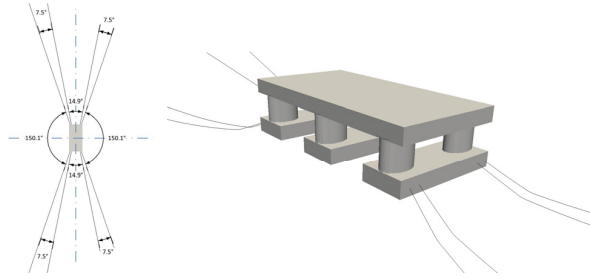


Fig. 4. Sketch (left) and configuration (right) of the mooring system

Table 2. Primary parameters of mooring system

Primary parameter	Unit	Value
Number of mooring lines		8
Angle between each group	°	150.1/14.9
Depth to anchors below SWL	m	10
Depth to fairleads below SWL	m	5
Equivalent mooring line mass in water	Kg/m	97.08
Diameter of each mooring line	m	0.095
Young's modulus	N/m <sup>2</sup>	$1.2 \times 10^{11}$

### Configuration of Computational domain and mesh

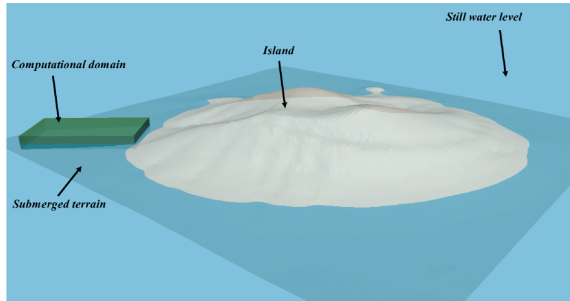


Fig. 5. Sketch of computational domain, island and submerged terrain.

The most significant work in this paper is to investigate the influence of the submerged terrain upon the wave evolution characteristics and the corresponding hydrodynamic response of the semi-submersible platform. Hence, the model of island and submerged terrain was built as shown in Fig. 5. The computational domain is posited by the island and the relevant water depth is 10 m and the submerged terrain was taken into account as the bottom boundary condition of the computational domain. The mesh of the computed domain and model are shown in Fig.6 (upper left). The solver used in this paper is based

on the OpenFOAM who provides users a very powerful and convenient utility named snappyHexMesh (OpenFOAM, 2013) to create the computational mesh with high quality in relatively short time, by which the mesh of the work was generated. The whole cell number of the computed domain that include the platform is 1.47 million and 1.57 million without the platform which is built for the wave evolution test. The terrain extracted from the island model which was adopted as the bottom boundary of the computational domain is shown in Fig. 6 (upper right), and the relevant irregular slope of the bottom can be seen in the lower left figure of Fig. 6. The local mesh of the platform is shown in the lower right corner. The configuration of the computational domain (wave direction, position of platform, wave absorption area (wave damping area) and the mooring lines) are shown in Fig.7.

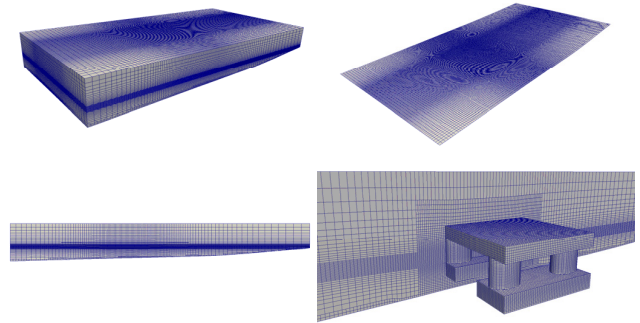


Fig. 6. Computational mesh of the domain (upper left), extracted terrain (upper right), lateral view of the domain (lower left) and the local view of the mesh beside the platform.

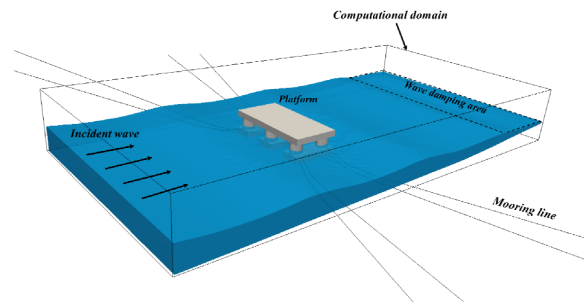


Fig. 7. Configuration of the computational domain with all key factors.

### Computational cases

The key problem of this paper is to discuss the wave. Herein, several different wave conditions were considered in this work, and all the wave cases implemented to calculate the RAO are extracted from the wave experimental test that conducted by Ding (2014). The wave cases are shown in Table 3 in detail. All the waves that generated in this study are all regular wave and belong to range of the Stokes 2<sup>nd</sup> wave theory as shown in Fig. 8. For the accuracy of the calculation of RAO, all the waves are adjusted and the wave height around the center of the platform was ensured to be about 2 m as the model test. So that, a wave propagation test is needed without platform to ensure the wave height and observe the wave evolution characteristics. This part is following in the results and discussion section.

Table 3. Wave condition implemented in this RAO calculation.

Wave cases	Wave height (m)	Wave period (s)
Case1	2	4.38
Case2	2	5.66
Case3	2	8
Case4	2	10.526
Case5	2	12
Case6	2	14
Case7	3	10.526

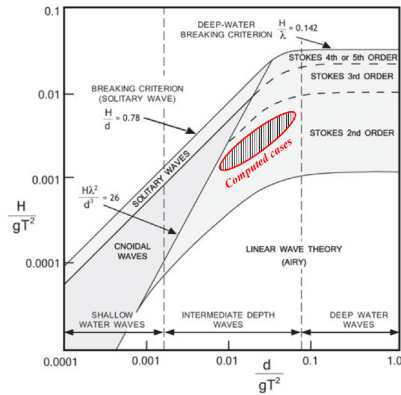


Fig. 8. Distribution of the computed cases in the wave theory diagram.

## RESULTS AND DISCUSSIONS

### RAO calculation and validation

RAO is a significant parameter in the hydrodynamic response investigation field, which is normalized value for the amplitude of a periodic response of a field variable divided by the amplitude of the regular wave (Coulling et al., 2013) and so that this dimensionless parameter can be adopted to evaluate the motion performance of the platform to the wave frequency/period. And in this section, the motion performance of the semi-submersible platform was calculated in each wave condition except the Case 7 that referred to in Table 3, and only the time-history line of Case 2 is given in Fig. 9 for the consideration of conciseness of the paper. The motion response of the platform in Case 2 given in this section is relative linear and some other cases may be nonlinear especially in pitch motion, which will be shown and analyzed in the future research. It is evident that the time-history lines of the motion of Case2 is relative steady, whereas the surge amplitude appears a nonlinear characteristic. The frequency of the surge motion is not only induced by the incident wave but also a larger period parameter. This motion is considered to be result of the low-frequency drift motion of the platform which is dominated by the low-frequency characteristics of the mooring system. For a further study of this phenomenon, a FFT (Fast Fourier Transform) is done to do a frequency-domain analysis. The transform results is also shown in Fig. 9 (lower-right). The first order peak of the line is the corresponding frequency of the incident wave whose period is 5.66s and frequency is 0.1767 Hz. And the second order peak is probably relevant to the natural period of the surge motion in terms of experiences which is just

an assumption that has not be validated. However, the validation work about free decay motion of these three degrees of motion is ongoing and will be presented in the future.

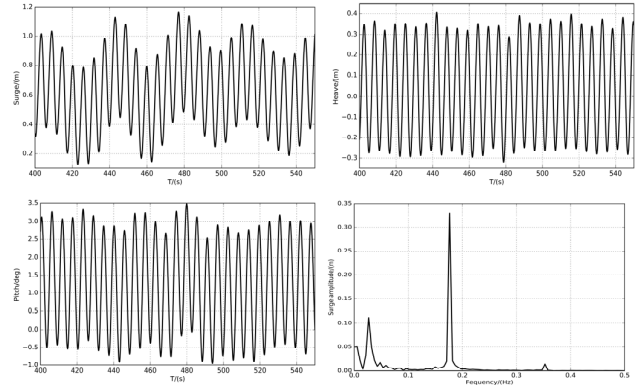


Fig. 9. Time-history result of three DOFs (Degree Of Freedom), surge (upper left), heave (upper right), pitch (lower left) and the FFT result of the surge motion (lower right).

The characteristic of the semi-submersible platform in the presence of regular waves has been investigated by calculation of RAO magnitudes. According to the International Towing Tank Conference (ITTC) that motion data should be collected at least for 10 quasi-steady cycles under regular wave conditions to ensure accuracy of results (ITTC, 2002). Herein, the RAO values presented are calculated from the average value of the nearly converged harmonic responses when the result is relatively steady. The RAO results are shown in Table 4, and the heave and pitch results that compared with the experimental test and AQWA calculation (Ding et al., 2014) are given in Fig. 10. AQWA is a popular numerical software which is based on the potential flow theory.

The computed results by the present numerical solver naoe-FOAM-SJTU show great agreement to the computational test as shown in Fig. 10. Moreover, most of the calculated results is better than the AQWA results which is based on the potential flow method, especially wave period is about 15 s in heave motion results and about 5 s in pitch motion. This is just the reason why CFD method is chosen in this study but not potential flow theory. The theory of potential flow is a mature theory which has been widely used in most issues in ocean engineering. It can capture most of interactions between floating body and waves except minor viscous effect, which neglects some aspects of the detailed hydrodynamics and incorporate the fluid effects on the structure via coefficients in the six degree-of-freedom (6-DOF) equations of motion that account for the pressure field due to the motion of the floater (added mass coefficient), damping effects (damping coefficient), buoyancy (restoring coefficient) and wave excitation force vector (Tran, 2015). Most of these influence are taken into account by given a semi empirical coefficient into the software whereas the CFD method take hydrodynamic parameter into account directly, so that the vortex and viscous can be well considered in the study which take a prominent part in the wave problems in shallow water and this is one of the possible reason that why CFD results are better than the AQWA. Some evident discrepancy can be easily captured between the CFD results and test data. It is probably the reason of absence of turbulence with laminar model and the imperfect of numerical method of mooring system. Moreover, the discrepancy may be caused by the scale effect for that the numerical calculation is carried out with real scale while model test with model scale. What else,

it is obviously that this platform is more sensitive to the low-frequency waves especially these whose period is 16-20 s. Whereas the platform is not very sensitive to the large-frequency waves which means that the motion performance of the platform is pretty good in natural environment near the island where the wave period is not very large exactly. Moreover, the figure of post-process of Case 3 is shown in Fig.11 which depicts the change of waveform, motion pattern and movement of mooring lines. It is obvious that the waveform has been prominently disturbed by the existence of the platform that the draft of the platform is almost half of the water depth which strongly limits the movement of water particles, so that the waveform changes. It is easy to capture the diffraction waves around the column of the platform which scour the columns evidently that has a great influence on it.

Table 4. Results of RAO in three DOFs.

Wave Cases	Case1	Case2	Case3	Case4	Case5	Case6
Surge RAO	0.10	0.34	0.76	1.41	2.39	1.12
Heave RAO	0.19	0.33	0.67	0.53	0.59	0.52
Pitch RAO	1.07	1.88	1.01	0.80	0.35	1.00

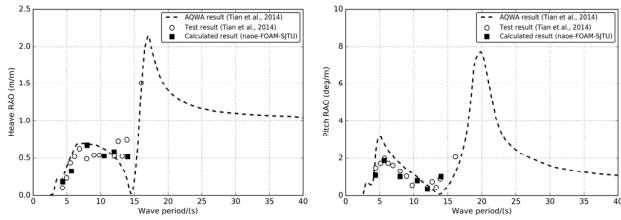


Fig. 10. Comparison of RAO results in heave (upper) and pitch (lower) between present work, Experimental test and the AQWA results.

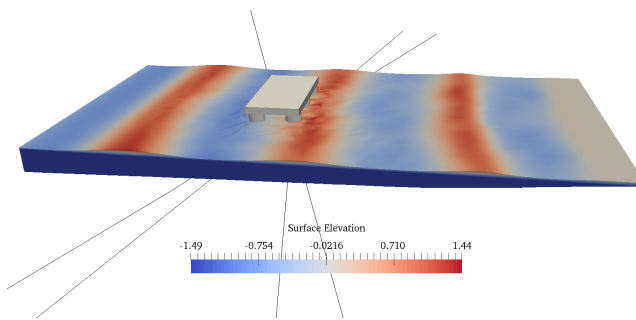


Fig. 11. Simulated hydrodynamic response result of Case 3.

### Wave evolution characteristics and hydrodynamic response of platform with different wave steepness

As mentioned in introduction part, wave steepness is a significant parameter in the shallow water wave evolution process, and according to the former analysis, different wave steepness may result in distinct wave feature and also different hydrodynamic performance of the floating structure. Wave steepness is the value that the wave height divided by the wave length, and according to the dispersion relation of certain water depth, wave length is calculated with respect to the wave period. So that, certain wave steepness can be expressed by wave height and period. In this part, different wave steepness are primarily

studied and the Case7 condition is calculated in this work whose wave period is 10.526 s which is equal to the Case 4 whereas the wave height is 3 m.

Wave evolution and breaking is a representative feature of shallow water waves, which is the results of the limitation of the impermeable bottom boundary condition to the movement of fluid particles. First of this section, wave propagation is primarily investigated without the influence of the platform, and the evolution process among the cases of Table 3 will be presented. In order to capture the waveform in the wave evolution process, 20 wave gauges were arranged in the computational domain as shown in Fig. 12. The center of the platform, which is should be but removed to prevent the disturbing upon the wave field, is marked in the Fig. 12, and it is also the position of the wave gauge No. 10. The wave gauges were serial numbered from the inlet side to the outlet side by No. 1 to No. 20.

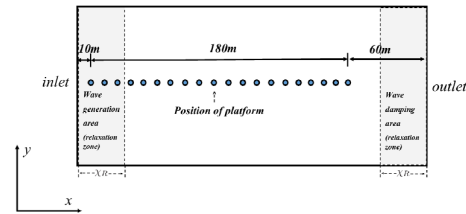


Fig. 12. Arrangement of the wave gauges in the computational domain.

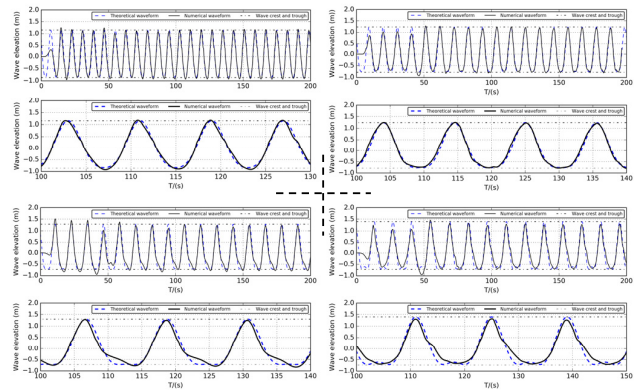


Fig. 13. Comparison between wave elevation time-history line at wave gauge 10 (position of platform) and the theoretical waveform with 10 m water depth in Case 3 (upper left), Case 4 (upper right), Case 5 (lower left) and Case 6 (lower right). (Each figure is composed of two subgraph that the upper is the long-time history line and the lower one is portion of the upper one drawn for an explicit analysis)

The wave generation work of the wave conditions Case1-6 in the Table 3 was firstly done to ensure that the wave height at the wave gauge 10 (position of the platform) is 2 m to support the implementation of RAO calculation in the corresponding wave condition. And the wave elevation time-history line at the gauge 10 of different wave cases are shown in the Fig. 13 with solid lines. At the same time, the numerical results are compared with the theoretical results of the waveform with dash lines which are calculated by the Eq. 3 which is the formula of Stokes 2<sup>nd</sup> wave. Also the value of wave crest and wave trough of the theoretical results are marked in the figure with dash-dotted lines. It is obvious that the waveform of the numerical results are similar with the theoretical results especially that the wave crest value and trough value agree to the theoretical value quite well. So that, the wave height is

ensured to be 2 m and the parameter of wave generation can be adopted into the calculation of RAO. Moreover, the value of the crest and trough also show the typical characteristic of Stokes wave that the absolute value of wave crest is greater than that of wave trough which is different from the Airy wave theory that the wave form is asymmetry about the still water level but with a higher crest and a more flat trough, and this characteristic has been greatly captured in the calculation. However, the waveform of the numerical results has evident discrepancy from the theoretical forms in some aspects especially in the Case 5 and Case 6. The wave crest trends to the front side of the waveform (left side in this picture) evidently which is absolutely the influence of the submerged terrain that the water particles accumulate to the front part of the wave crest in the process of wave evolution. The possible reason of the discrepancy is that the theoretical equation is deduced upon the assumption of flat bottom condition in which wave evolution is not considered.

For a further exploration of the effect of the irregular slope of the submerged terrain on the wave evolution process, Fig.14 was drawn to dissect the transformation of the waveform in the propagation process. The depiction of submerged terrain and different waveform lines were drawn in the figure for different cases whose wave period is 8 s, 10.526 s, 12 s and 14s in Fig.14 (left). The data of these lines were extracted from the center line of the free surface ( $y = 0$ ) of each numerical case and so that to analyze the wave evolution phenomenon along the wave propagation direction (x-axis). The evolution feature of waveform is more clearly to be captured through this figure that wave height increases evidently in the process of propagation from -13 meter depth to -4 meter depth. After that, the submerged terrain was removed for an explicit sketch as seen in Fig. 14 (right). It is evident that the second peaks of all the cases are greater than the first one especially when  $T=12$  and  $T=10.526$ . With the reduction of the water depth, the velocity of the wave decreases and so that the speed of wave front is slower than the rear part that causes the accumulation of water particles at the wave crest and also the wave crest trends to the front part of the wave. So that, it can be easily captured from the figure that the value of wave crest increases and the wave crest trends to the front part when the water depth decreases. If the wave height is large enough or that the waveform is more asymmetry, the water particles cannot maintain the waveform anymore and the wave may turning and breaking.

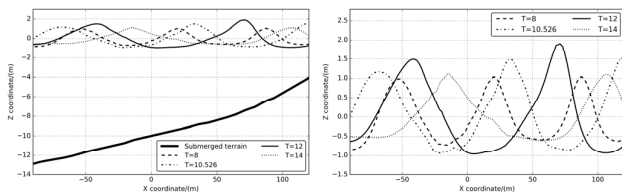


Fig. 14. Whole sketch (left) and explicit sketch (right) of waveforms along the x-axis of different wave cases at a fixed certain time.

Moreover, the wave evolution phenomenon can be also captured from the Fig. 15 which is the elevation distribution of the free surface of the Case 6. The shape of crest line 2 in the figure is different from that of line 1 that it transfer from a straight line into a bent one which is also a typical phenomenon of wave evolution near the shoreline. The probable reason is that the bottom is not flat and the center of which is deeper than the both side so that the wave velocity is greater in the center line which leads to the bent crest line. As mentioned above, the wave velocity will change in the pace of the water depth and the wave will refract, so that the wave crest is always parallel to the shoreline in daily life. To validate this explanation, a further work was done as seen in

Fig. 16 (left) which is the free surface elevation of Case 3 that the data along the wave crest line and wave trough line were extracted and depicted in the right figure. The solid line is the wave crest data along the y-axis and the dash line is the wave trough data. Both of the two lines fluctuate around the mean value of the wave crest and trough. It is exactly the result of the rough bottom that wave propagation appears a three dimensional characteristic and so that the color alone the two lines is not the same degree in the left figure. Moreover, it is interesting that the Fig. 15 and Fig. 16 (left) show an evident discrepancy that the wave crest line of the former one is bent but the latter one does not. The only difference between the two cases is the wave steepness ( $H/L$ ). So that the investigation upon the wave steepness will be conducted.

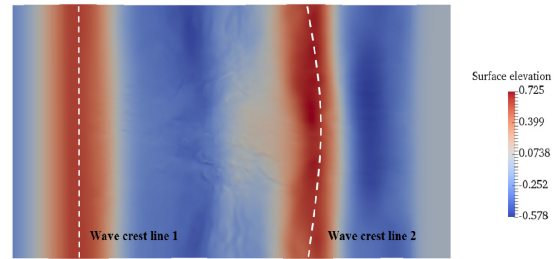


Fig. 15. Wave crest lines of the wave at certain time of Case 6 ( $T=14$  s).

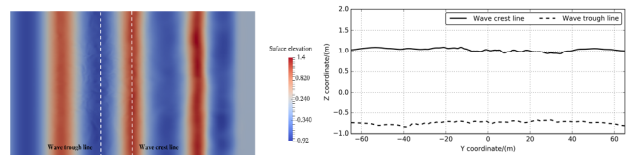


Fig. 16. Free surface elevation of Case 3 (left) and the wave crest and trough lines (right) along the dash line in the left figure.

As shown in Fig. 17-19, the waveform measured by different wave gauges of different cases are presented. The four wave gauges are arranged along the x-axis as shown in Fig. 12, so that the data measured can respectively be depicted into the wave evolution feature. It is evident that wave evolves and changes in all the process in each case. The difference between Fig. 17 and Fig. 19 is that the wave height of Fig. 17 is 2 m and latter one is 3 m. Although the little change, great influence occurs. With the increase of the wave height, the phenomenon of the rise of wave crest is more clear that wave crest of gauge 12 is more than 1.8 m. what's more, it will be higher with the reduction of water depth as to that the wave steepness exceeds the limit of wave breaking criterion, and so that the wave breaking occurs as shown in Fig. 19 (right). The wave is obviously turning and breaking, and waveform cannot maintain a smooth shape. There are several criterions about the critical wave breaking. One of the most popular criterion is that the wave breaking occurs while the wave steepness exceeds the limit that  $H/L$  (Height/Length) is greater than 0.142 (Tsai, 2005). So that it is the reason why the wave of Case 7 breaks and it is also the reason of that the largest crest of Case 5 (Fig. 18) is just about right the largest crest value of Case 7 but no wave breaking (the wave length of Case 5 is larger).

Wave breaking is an air-sea interaction that mass, momentum and energy transfer between these two phases. It is evident in the Fig. 19 (left) that wave height of gauge 12 is relative large and following that the wave form of gauge 17 has transformed seriously, and by the time

that the wave propagate to gauge 20, the wave height is actually small and the wave breaks completely. This is just because that the wave energy has absolutely dissipate from potential energy to kinetic energy in the process of wave breaking. The breaking wave in the Fig. 19 (right) has been marked and another interesting phenomenon can be observed that an interference wave has been simulated at the position of wave trough which is never found in any other cases. So that a reasonable assumption is proposed that the small interference fluctuation is derived during the breaking process that the return flow is created seaward in order to balance the shoreward mas flux created in the overturning wave crest. The interaction between the incoming breaker in the upstream side and the seaward return flow of the preceding wave from the downstream side strongly influences the breaking process and thus the characteristics of the wave field (Chella, 2015).

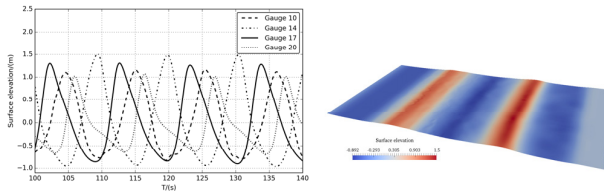


Fig. 17. Waveform (left) measured by different wave gauges (No. 10, No. 14, No. 17 and No 20) and feature of free surface (right) of Case 4.

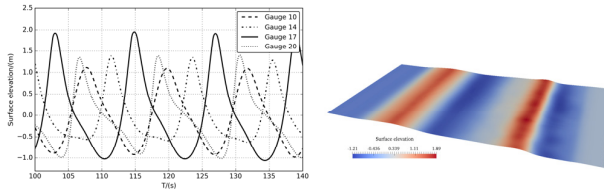


Fig. 18. Waveform (left) measured by different wave gauges (No. 10, No. 14, No. 17 and No 20) and feature of free surface (right) of Case 5.

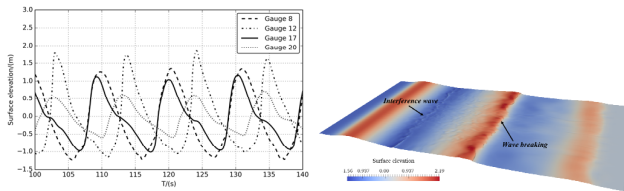


Fig. 19. Waveform (left) measured by different wave gauges (No. 8, No. 12, No. 17 and No 20) and feature of free surface (right) of Case 7.

The influence of different steepness may results in different wave evolution characteristics and thereby has great influence on the hydrodynamic characteristics of the platform. As shown in Fig 20, the illustration are about Case 7 (left) and Case 4 (right) who have the same wave period and length but different wave height. The upper rows of figure is at the time that the wave crest arrives the first row of the columns of the platform, and it is evident that a small wave run-up has occurs in Case 7 while the wave feature of the right one is relative flat. From the middle row of the Fig. 20, it is evident from the left figure that the first row of columns has significant effects on the wave field that the elevation between the two rows of columns rise mightly which is higher than that around the first row. It is the result of the interference of wave surface between the two rows of columns. Finally,

the lower row of the Fig. 20 is the time when the wave crest is going to leave the second row of columns. It is clear that there exists a second wave peak that caused by the accumulation of water particles, influence of submerged pontoons and intricacy of wave field. The comparison shows great divergence between the two cases who has different wave steepness that the wave surface of Case 7 is more intricate and non-linear whereas Case 5 is relatively gentle and linear.

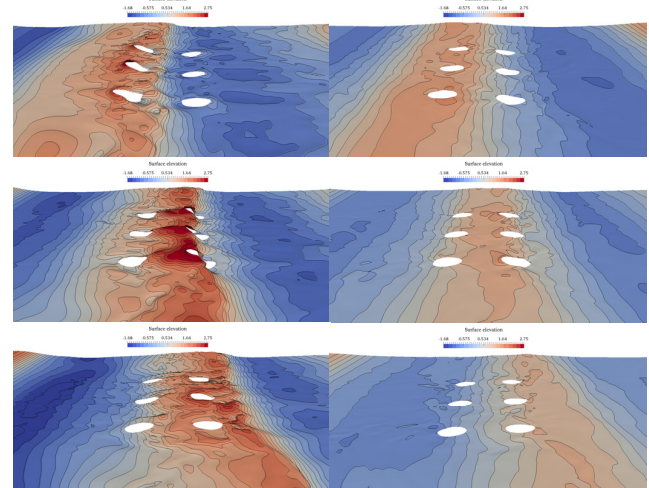


Fig. 20. Comparison between elevation of free surface of Case 7 (left) and Case 4 (right) at different time steps that wave crest arrives the first row of columns (upper), wave crest arrives the second row of columns (middle) and wave crest leaves the second row of columns (lower).

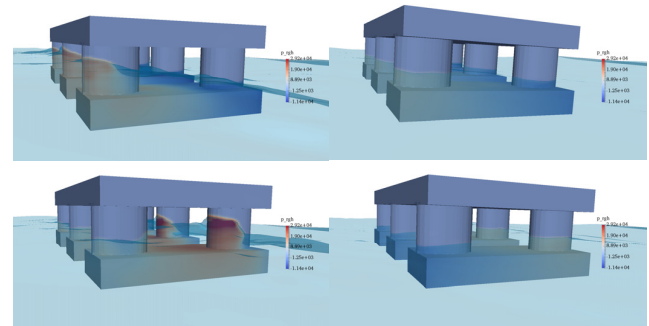


Fig. 21. Comparison between dynamic pressure of Case 7 (left) and Case 4 (right) at different time steps that wave crest arrives the first row of columns (upper), crest arrives the second row of columns (lower).

Meanwhile another comparison was done as seen in Fig. 21 that the dynamic pressure distribution of the platform is compared. The left array is about Case 7 and the right array is about Case 5, and the upper row is at the time that the wave crest arrives the first row of columns and the lower row is that arrives the second row of columns. It is evident that the wave run-up phenomenon occurs in the Case7 which has a large wave steepness and meanwhile the dynamic pressure that acting on the platform by the wave is relative greater compared with the Case 5 in which the dynamic pressure is small with no wave run-up. Slamming phenomenon also occurs in this process in Case 7 which deserve a further study in the future.

## CONCLUSIONS

The numerical simulation of hydrodynamic response of a semi-submersible platform and the wave evolution characteristics research with a submerged terrain in shallow water near island have been carried out using our in-house two-phase flow CFD solver naoe-FOAM-SJTU. Stokes wave theory is adopted in the generation of waves, and the purpose of the present study is to investigate the influence of the irregular slope of the submerged terrain upon the wave evolution and the motion response of the platform. It has been shown that the numerical results of RAOs of the motion performance of the semi-submersible platform show great correlation to the experimental test results which is better than the results of AQWA who is based on the potential flow theory. Some analysis has been done to explain the discrepancy between the CFD result, test data and AQWA results. Subsequently, the effect of wave steepness upon wave evolution investigation and floating platform was carried out and comparison between numerical waveform and theoretical waveform was conducted. Meanwhile the waveform along the propagation direction was extracted from the free surface of the results and a more intuitive results about the wave evolution process were presented. In this part, the influence of the irregular terrain upon the waveform was also discussed and the refraction phenomenon of the wave crest line has been also captured in the study. Moreover, it is shown that wave steepness has significant effect on the wave evolution. In this part, wave breaking occurs in the calculation of Case 7, and then a series of analysis were carried out around the wave breaking phenomenon. Meanwhile, the comparison of the hydrodynamic characteristics of the platform between Case 7 and Case 5 was done. Some strong nonlinear phenomenon has been captured such as wave run-up and slamming in Case 7 whose fluid field is more intricacy. Also the interference phenomenon between the two rows of columns has been observed and wave elevation rises mightily between the two columns. All the work conducted in the present study validates the accuracy and reliability of the naoe-FOAM-SJTU solver and the wave evolution characteristics and hydrodynamic study has been analyzed explicated. Notwithstanding, there still exists some problems just like the nonlinear analysis of slamming and motion performance of the platform in breaking waves need to be well investigated in the future.

## ACKNOWLEDGEMENTS

This work is supported by the National Natural Science Foundation of China (51379125, 51490675, 11432009, 51579145), Chang Jiang Scholars Program (T2014099), Shanghai Excellent Academic Leaders Program (17XD1402300), Shanghai Key Laboratory of Marine Engineering (K2015-11), Program for Professor of Special Appointment (Eastern Scholar) at Shanghai Institutions of Higher Learning (2013022), Innovative Special Project of Numerical Tank of Ministry of Industry and Information Technology of China(2016-23/09) and Lloyd's Register Foundation for doctoral student, to which the authors are most grateful.

## REFERENCES

Banner, M, Peregrine, DH (1993). "Wave breaking in deep water". *Annu Rev Fluid Mech*, 373–397.

Basco, DR (1985). "A qualitative description of wave breaking". *J Waterw Port Coast. Ocean Eng*, 3, 171–188.

Blenkinsopp, C, Chaplin, J (2008). "The effect of relative crest submergence on wave breaking over submerged slopes". *Coast Eng*, 55, 967–974.

Chella, MA, Bihs, H and Myrhaug, D (2015). "Characteristics and profile

asymmetry properties of waves breaking over an impermeable submerged reef". *Coast Eng*, 100 (2015) 26–36.

Cokelet, E (1977). "Breaking waves". *Nature* 267, 769–774.

Coulling, AJ, Goupee, AJ, Robertson, AN, Jonkman, JM and Dagher, DJ (2013). "Validation of a FAST semi-submersible floating wind turbine numerical model with DeepCwind test data". *J Renew Sustain Energy*, 5(2): 023116.

Ding J, Tian C, Zhang, K and Wu B (2014). "Study on Motion and Load Responses of Semi-submersible Platform near Islands and Reefs". *Proc 13st Natl HydroDyn Academic Conf*, Qing Dao, China, 1159-1166. (in chinese)

Donley, MG and Spanos, PD (1992). "Stochastic response of a tension leg platform to viscous and potential drift forces". *Proc 11th Int Offshore Mech and Arctic Engineering Conf*, ASME, New York, NY, Vol. II, pp. 325-334.

Frank, Lee DY and Choi YH (2005). "An Experimental Study on the Extreme Motion Responses of a SPAR Platform in the Heave Resonant Waves". *Proc 15th Int Offshore Polar Engineering Conf*, Seoul, Korea, ISOPE, (1).

ITTC (2002). ITTC Recommended Procedures – Sea Keeping Experiments. 2002: 4.

Jacobsen, NG, Fuhrman DR and Freds  $\phi$ e (2012). "A wave generation toolbox for the open-source CFD library: OpenFoam". *Int J Numer Method Fluid*. 70:1073–1088.

Kobayashi, M, Shimada, K and Fujihira, T (1987). "Study on dynamic response of a TLP in waves". *J Offsho. Mech Arctic Engng*, 109, 61–66.

Lee, YW, Incecik, A, Chan, HS and Kim, ZK (2005). "Design Evaluation in the Aspects of Hydrodynamics on a Prototype Semi-Submersible with Rectangular Cross-Section Members". *Proc 15th Int Offshore Polar Engineering Conf*, Seoul, Korea, ISOPE, 3, 315-328.

Liu, Y, Peng Y and Wan D (2015), "Numerical Investigation on Interaction Between a Semi-Submersible Platform and its Mooring System", *Proc ASME 2015 34th Int Conf Ocean Offshore Arctic Eng*, May 31-June 5, 2015, St. John's, Newfoundland, Canada, OMAE2015-412948

Maeda, H, Jo, HJ and Miyajima, S (1992). "Effects of directional waves on the low-frequency motions of moored floating structures". *Proc Second Int Offshore and Polar Engng Conf*, ISOPE, San Francisco, ISOPE, Vol. 3, pp. 489-495.

Morison, JR, Johnson, JW and Schaaf, SA. (1950). "The force exerted by surface waves on piles". *J Pet Technol*, 2(5), 149-154.

OpenFOAM. Mesh generation with the snappyHexMesh utility. (2013). Available from: <http://www.openfoam.org/docs/user/snappyHexMesh.php#x26-1510005.4>.

Peregrine, DH (1983). "Breaking waves on beaches". *Annu. Rev Fluid Mech*, 149–178.

Perlin, M, Choi, W, Tian, Z (2013). "Breaking waves in deep and intermediate waters". *Annu Rev Fluid Mech*, 115–145.

Shen, Z, Zhao, W, Wang, J and Wan, D. (2014). "Manual of CFD solver for ship and ocean engineering flows: naoe-FOAM-SJTU". *Technol Rep Solver Man*, Shanghai Jiao Tong University.

Takikawa, K, Yamada, F and Matsumoto, K (1997). "Internal characteristics and numerical analysis of plunging breaker on a slope". *Coast Eng*, 31, 143–161.

Tian, C, Ding, J and Wu, Y (2014). "Experimental Investigations on Hydrodynamic Responses of Floating Platform near Island". *Proc 13st Natl HydroDyn Academic Conf*, Qing Dao, China, 472-480. (in chinese)

Ting, FCK, Kim, YK (1994). "Vortex generation in water waves propagating over a submerged obstacle". *Coast Eng*, 24, 23–49.

Tran, TT, Kim, DH (2015). "The coupled dynamic response computation for a semi-submersible platform of floating offshore wind turbine". *J Wind Eng Ind Aerodyn*, 147:104–119.